Advances in Applied Mathematics and Mechanics
Adv. Appl. Math. Mech., Vol. **17**, No. 1, pp. 240-262

DOI: 10.4208/aamm.OA-2022-0250
February 2025

The Boundary Mapped Collocation Method for Heat Conduction Problems with Heat Generation Spatially Varying Conductivity

Zhentian Huang[1,2,3,*], Dong Lei[3], Zi Han[4], Heping Xie[2] and Jianbo Zhu[2]

[1] *School of Civil Engineering & Architecture, East China Jiaotong University, Nanchang, Jiangxi 330013, China*
[2] *Guangdong Provincial Key Laboratory of Deep Earth Sciences and Geothermal Energy Exploitation and Utilization, Institute of Deep Earth Sciences and Green Energy, College of Civil and Transportation Engineering, Shenzhen University, Shenzhen, Guangdong 518060, China*
[3] *College of Mechanics and Materials, Hohai University, Nanjing, Jiangsu 211100, China*
[4] *College of Civil Engineering and Architecture, Nanchang Hangkong University, Nanchang, Jiangxi 330063, China*

Received 26 September 2022; Accepted (in revised version) 24 September 2023

Abstract. In this paper, the boundary mapped collocation (BMC) approach is presented for the analysis of heat conduction problems involving heat generation and non-homogeneous thermal conductivity. The proposed methodology is introduced to produce the numerical solutions of the temperature field within the framework of the BMC method, a novel boundary meshless method, without resorting to requiring any integral calculation, neither in the domain nor at the boundary. In particular, the arrangement of discrete nodes is restricted to the axis, which brings the spatial dimension down by one. The technique also reduced the traditional complex shape functions to succinct one-dimensional boundary shape functions by using one-dimensional basis functions and weight functions for two- and three-dimensional approximation implementation. In addition, four numerical applications and comparisons with the outcomes of the finite element approach and another meshfree method are used to demonstrate the correctness, convergence, and stability of the BMC method.

AMS subject classifications: 80M22, 65-04, 68-04

Key words: Boundary mapped collocation method, heat conduction, heat generation, spatially varying conductivity, meshless method.

*Corresponding author.
Email: zhentian_huang@163.com (Z. Huang)

1 Introduction

One of the most significant jobs for the scientific and industrial communities has always been the thorough investigation of heat transport issues through the solution of various partial differential equations in numerous engineering domains. Particularly, the heat conduction issues of functionally graded materials (FGM) with anisotropic mechanical properties have been receiving increasing attention for decades. However, analytical solutions for these heat conduction issues are hardly ever developed because of the variability of the material. As a result, computer-based techniques have been widely used in the study of heat conduction. The entire discretization of the computation domain is not necessary when using domain discretization techniques like the finite difference method (FDM) [1], finite volume method (FVM) [1], and finite element method (FEM) [2, 3] to solve these problems. The fundamental drawback of domain discretization techniques is the complexity of shape mesh production, which is computationally expensive. In addition, the boundary element method (BEM) [4–8] has been proposed as an effective alternative to the discretization of the boundary over the boundary.

Although the aforementioned methods have been applied to conduct heat transfer analysis successfully, they inherently own several drawbacks. The FEM, as one of the most popular numerical methods, resorts to the generation mesh using a polynomial representation for approximation of the solution region. Nevertheless, due to the C^0 continuous of the FEM shape function [9, 10], the mesh generation not only is time-consuming but also leads to the error with complex geometrical shape discretization. Also, since domain integrals are included in the integral equations, the main challenges faced by the BEM are the costly numerical integrations and computational expenses for an irregular region meshing [11, 12]. To circumvent the disadvantage of mesh generation, an alternative referred to as the meshfree method, such as large deformation, high gradient, and discontinuities.

In recent years, numerous meshless methods have been proposed to promote the achievement of approximate solutions for heat conduction analyses systematically. Sigh et al. [13] introduced the element-free Galerkin (EFG) method to analyze transient nonlinear thermal conduction within a solid structure. Zhang et al. [14] improved the EFG method for analyzing isotropic thermal conductivity. Gao [11] proposed the meshless BEM to analyze heat conduction with anisotropic thermal conductivity. Cui et al. [15] proposed the radial integration polygonal boundary element method (RIPBEM) for thermal conduction analyses with complex 3D geometries. Wu and Tao [16] employed the meshless local Petrov-Galerkin (MLPG) method to analyze steady-state thermal conduction with complicated boundary conditions. Li et al. [17] analyzed thermal conduction by combining the MLPG and FVM methods within two-dimensional irregular geometry. Hidayat [16] presented a meshless finite difference approach with B-splines technique for solving coupled advection-diffusion-reaction problems.

However, since these weak-form methods could not get rid of a grid generation with numerical integration, the above EFG, BEM, and MLPG methods are not complete mesh-

less approaches. Hence, the improvement is to establish the approximate form of the strong type of governing equations by introducing the collocation technique. For the sake of constructing the strong-form approximation for the governing equations, the PDEs are approximated by numerous discrete nodes within the solution domain. Atluri et al. [18–20] presented the collocation of Dirac's Delta function as the test function, in which no integration is required. Wei and Chen et al. [21]extended the singular boundary method (SBM) to thermal conductivity analyses of nonhomogeneous materials. Dai et al. [22] proposed the weighted least-squares collocation method (WLSCM) for solving heat conduction problems within two and three-dimensional irregular domains. The previous research results indicated that meshless methods have become an effective alternative to classical FEM and BEM due to some distinct advantages such as high-order continuous shape functions, no mesh alignment, and easy implementation of h-adaptivity.

It is noted that time-consuming is a serious drawback within the meshless methods, especially weak-form approaches. For improving the computational efficiency, a recent boundary-type meshless collocation technique, referred to as the boundary mapped collocation (BMC) method or the boundary moving least squares method (BMLS), has been presented to solve the wave propagation, 2D elastic dynamics, and 3D elastic static problems [23–26]. The BMC method does not require any integral neither in the domain nor on the boundary. Hence, its computational efficiency is higher than the weak-form-based meshless techniques. Especially, only one-dimensional moving least squares shape functions and their derivatives are adopted to solve higher-dimensional problems in BMC approximation, which greatly simplifies the process of calculation. Additionally, the BMC method possesses the Kronecker delta property since the substitution method is introduced to apply the essential or/and natural boundary conditions.

In this context, the BMC method is developed in the present study for the isotropic heat conduction analyses with heat generation spatially varying conductivity in a two-dimensional or three-dimensional domain. The brief outline of this paper is as follows: Firstly, the heat conduction problems are reviewed in Section 2. The derivation process of the BMC method is represented in Section 3. Section 4 investigates the accuracy and efficiency of the BMC approach through four numerical examples. The discussions of numerical results are shown in Section 5. Section 6 represents the conclusions of this study in the end.

2 Problem definition

Consider an anisotropic steady-state heat conduction problem with heat generation and spatially varying thermal conductivity, contour Γ, and domain Ω. The governing partial equation concerning the temperature T is represented as

$$\nabla\cdot(\mathbf{k}\nabla T)+Q=0 \quad \text{in} \quad \Omega. \tag{2.1}$$

Subjected to the boundary conditions, which are defined as follows

$$T=\bar{T} \qquad \text{on} \quad \Gamma_1, \tag{2.2a}$$

$$q=(\mathbf{k}\nabla T)\cdot\boldsymbol{n}=\bar{q} \qquad \text{on} \quad \Gamma_2, \tag{2.2b}$$

$$(\mathbf{k}\nabla T)\cdot\boldsymbol{n}=h\left(T_f-T\right). \tag{2.2c}$$

In Eqs. (2.1)-(2.2b), $\mathbf{k}=\text{diag}(k_x,k_y,k_z)$ is the tensor of thermal conductivity, $\text{W}/(\text{m}^\circ\text{C})$, T is the temperature, Q is the heat sink/source, $\bar{T}$ is the initial temperature, q is the normal heat flux on Γ_2, $\bar{q}$ is the prescribed heat flux, and $\boldsymbol{n}$ is the unit vector outward normal to Γ_2.

3 Boundary mapped collocation approximation

3.1 Moving least squares approximation

In the BMC approach, one-dimensional boundary shape functions and their derivatives, which are derived employing the moving least squares (MLS) technique, are adopted to construct the three-dimensional approximation space of the field variable u. As the basics of the BMC approach, a short introduction to the MLS method is given in this part. Considering an unknown function $u(x)$ for an arbitrary domain Ω, which is approximated by a polynomial expansion within a small support domain Ω_0 of numerous random discrete nodes. The approximate equation $\hat{u}(x)$ at each computational point is defined as follows

$$u(x)\cong\hat{u}(x)=\sum_{i=1}^{k}p_i(x)\alpha_i=\mathbf{p}(x)^T\boldsymbol{\alpha}=\mathbf{N}\mathbf{u}, \tag{3.1}$$

where coefficients $\boldsymbol{\alpha}(x)=[\alpha_1,\alpha_2,\cdots,\alpha_k]^T$, and vector $\mathbf{p}(x)$ is a complete monomial basis of order k containing typically monomials within the two/three-dimensional space coordinates. The linear base polynomials $\mathbf{p}^T(x)=[1,x]$, $(k=2)$, and the quadratic base polynomials $\mathbf{p}^T(x)=\left[1,x,x^2\right]$, $(k=3)$ are adopted for one-dimensional space. The approximation functions can be written as follows in the matrix

$$\mathbf{u}=\begin{bmatrix}\hat{u}_1\\ \hat{u}_2\\ \vdots\\ \hat{u}_m\end{bmatrix}=\begin{bmatrix}\mathbf{p}_1^{\mathrm{T}}\\ \mathbf{p}_2^{\mathrm{T}}\\ \vdots\\ \mathbf{p}_{\mathbf{m}}^{\mathbf{T}}\end{bmatrix}\boldsymbol{\alpha}=\mathbf{C}\boldsymbol{\alpha}. \tag{3.2}$$

The coefficient $\boldsymbol{\alpha}(x)$ can be obtained by calculating the minimum for a weighted discrete L_2 norm at any computational point, which is given as follow

$$J=\sum_{I=1}^{m}\omega_j(x)\left[\hat{u}(x,x_I)-u(x_I)\right]^2, \tag{3.3}$$

where $\omega_j(x)$ is the weight function of the support domain at the discrete node x_j with $\omega(x)>0$, m is the corresponding quantity of discrete nodes in the support domain Ω_0.

As regards the unknown coefficients $\boldsymbol{\alpha}(x)$, it could be deduced as follows

$$\frac{\partial J}{\partial \alpha_i(x)}=0. \tag{3.4}$$

Then, the linear equations system of the coefficient $\boldsymbol{\alpha}(x)$ can be yielded as

$$\mathbf{A}(x)\boldsymbol{\alpha}(x)=\mathbf{B}(x)\mathbf{u} \tag{3.5}$$

and the coefficient vector $\boldsymbol{\alpha}(x)$ is rewritten as

$$\boldsymbol{\alpha}=\mathbf{C}^{-1}\mathbf{u} \quad \text{with} \quad \mathbf{C}^{-1}=\mathbf{A}^{-1}\mathbf{B}, \tag{3.6}$$

where

$$\mathbf{A}(x)=\sum_{j=1}^{m}\omega_j(x)\mathbf{p}\left(x_j\right)\mathbf{p}^{\mathrm{T}}\left(x_j\right), \tag{3.7a}$$

$$\mathbf{B}(x)=[\omega_1(x)\mathbf{p}(x_1),\omega_2(x)\mathbf{p}(x_2),\cdots,\omega_m(x)\mathbf{p}(x_m)]. \tag{3.7b}$$

Substituting Eqs. (3.6) and (3.8) into Eq. (3.1), the MLS shape functions can be represented as

$$\boldsymbol{N}(x)=\mathbf{p}^T(x)\mathbf{C}^{-1}=\mathbf{p}^T(x)\mathbf{A}^{-1}(x)\mathbf{B}(x). \tag{3.8}$$

Meanwhile, the first-order and second-order derivatives of the MLS shape function are given as

$$\frac{dN}{dx}=\mathbf{A}^{-1}\frac{dp}{dx}\mathbf{B}, \tag{3.9a}$$

$$\frac{d^2N}{dx^2}=\mathbf{A}^{-1}\frac{d^2p}{dx^2}\mathbf{B}. \tag{3.9b}$$

Moreover, the exponential function, the Gaussian function and the cone weight function are introduced to numerical simulations by the BMC approach in this study, which is given as follows

$$\omega(r)=\begin{cases}\dfrac{\exp\left(-r^2\beta^2\right)-\exp\left(-\beta^2\right)}{1-\exp\left(-\beta^2\right)}, & r\le 1,\\ 0, & r>1,\end{cases} \tag{3.10a}$$

$$\omega(r)=\begin{cases}1-6r^2+8r^3-3r^4, & r\le 1,\\ 0, & r>1,\end{cases} \tag{3.10b}$$

$$\omega(r)=\begin{cases}\dfrac{2}{3}-4r^2+4r^3, & r\le \dfrac{1}{2},\\ \dfrac{4}{3}-4r+4r^2-\dfrac{4}{3}r^3, & \dfrac{1}{2}<r\le 1,\\ 0, & r>1,\end{cases} \tag{3.10c}$$

where $r=|x-x_i|/d_m$ is the boundary value of the region in which the weight functions $\omega(r)>0$, $d_m=c\times dx$ is the radius of support domain Ω_0, dx is the distance between two discrete nodes, and the scale parameter c is the half number of points within the support domain Ω_0.

3.2 Boundary mapped collocation for three-dimensional heat conduction analyses

In this section, the BMC technique is introduced for the three-dimensional steady-state thermal conduction analyses in anisotropic materials with spatially varying thermal conductivity. The governing equation is expressed as

$$k_1\frac{\partial^2 T}{\partial x^2}+\frac{dk_1}{dx}\frac{\partial T}{\partial x}+k_2\frac{\partial^2 T}{\partial y^2}+\frac{dk_2}{dy}\frac{\partial T}{\partial y}+k_3\frac{\partial^2 T}{\partial z^2}+\frac{dk_3}{dz}\frac{\partial T}{\partial z}+Q(x,y,z)=0, \tag{3.11}$$

where T is the temperature at each computational point, k_1, k_2 and k_3 are variable thermal conductivity coefficient in the x, y, z direction, respectively. The three-dimensional solution domain Ω is discreted by the BMC implementation, as depicted in Fig. 1. It is noted that the BMC discretization is mapped by one-dimensional support domain compared with the MLS method (as shown in Fig. 2). Specially, the regular tensor product nodes are generated automatically by the proposed method. Hence, based on the BMC method, the temperature $T(x,y,z)$ at computational points which contain the tensor product nodes and boundary discrete nodes within the solution domain Ω is represented as

$$T(x,y,z)\cong\widehat{T}(x,y,z)=\sum_{i=1}^{k}p_i(x,y,z)\alpha_i=\mathbf{p}(x,y,z,t)^T\boldsymbol{\alpha}=\mathbf{N}(x,y,z)\widehat{\mathbf{T}}, \tag{3.12}$$

where $\mathbf{N}$(x,y,z) is the three-dimensional shape function of the BMC approach, and $\mathbf{N}(x,y,z)$ is established by one-dimensional shape functions $\mathbf{N}(x)$, $\mathbf{N}(y)$, and $\mathbf{N}(z)$ as follows

$$\mathbf{N}(x,y,z)=\mathbf{N}(x)\otimes\mathbf{N}(y)\otimes\mathbf{N}(z), \tag{3.13}$$

where $\mathbf{N}(x)$, $\mathbf{N}(y)$, and $\mathbf{N}(z)$ are formally equal to the one-dimensional MLS shape function, the detailed derivation process of space shape function $\mathbf{N}(x,y,z)$ is given in literature (Huang et al., 2019a; Huang et al., 2019b; Huang et al., 2020), and the symbol $\otimes$ represents the Kronecker of a matrix, also referred to as the tensor product operation, which is represented by the following form

$$\mathbf{H}_{(m_1\times m_2)}\otimes\mathbf{G}_{(m_3\times m_4)}=\begin{bmatrix} h_{1,1}g_{1,1} & \cdots & h_{1,m_2}g_{1,m_4} \\ \vdots & \ddots & \vdots \\ h_{m_1,1}g_{m_3,1} & \cdots & h_{m_1,m_2}g_{m_3,m_4} \end{bmatrix}, \tag{3.14}$$

where $\mathbf{H}$, $\mathbf{G}$ are m_1 by m_2 matrix and m_3 by m_4 matrix, respectively.

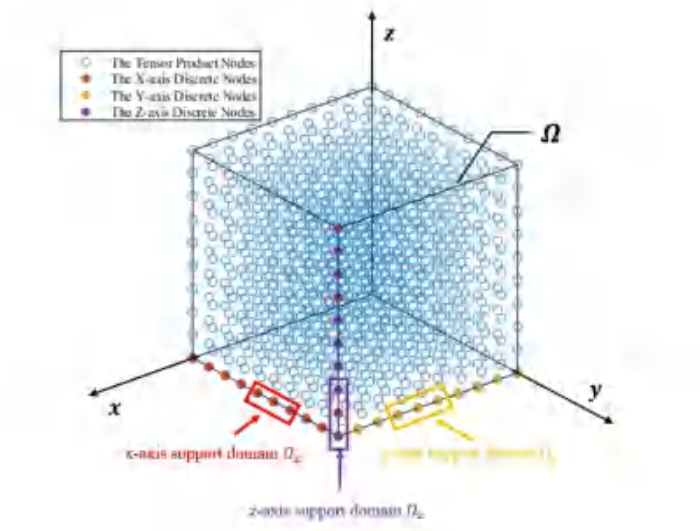

Figure 1: The weight function support domain of the BMC approximation in the three-dimensional solution domain Ω, Ω_x is a support domain of the x-axis, Ω_y is a support domain of the y-axis, Ω_z is a support domain of the z-axis.

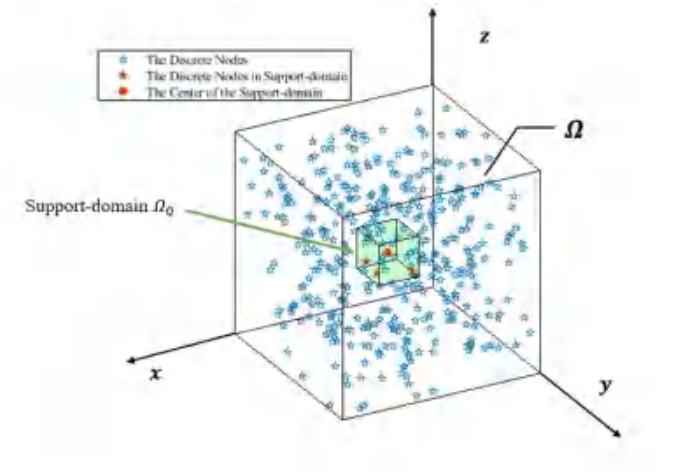

Figure 2: The weight function support domain of the MLS approximation in the three-dimensional solution domain Ω, Ω_0 is a support domain.

Further, the boundary shape functions $\mathbf{N}(x)$, $\mathbf{N}(y)$, and $\mathbf{N}(z)$ are written as $\mathbf{N}_1$, $\mathbf{N}_2$, $\mathbf{N}_3$ for brevity. Additionally, the corresponding first derivatives of shape functions are expressed as $\mathbf{N}_1^{(1)}$, $\mathbf{N}_2^{(1)}$, $\mathbf{N}_3^{(1)}$. Substituting Eq. (3.12) into Eq. (3.11), the discretization of

governing equation is given as follow

$$\begin{aligned}&\Big[k_{1,x}\cdot\mathbf{N}_1^{(1)}\otimes\mathbf{I}_2\otimes\mathbf{I}_3+k_1\cdot\mathbf{N}_1^{(2)}\otimes\mathbf{I}_2\otimes\mathbf{I}_3+k_{2,y}\cdot\mathbf{I}_1\otimes\mathbf{N}_2^{(1)}\otimes\mathbf{I}_3+k_2\cdot\mathbf{I}_1\otimes\mathbf{N}_2^{(2)}\otimes\mathbf{I}_3\\&\quad+k_2\cdot\mathbf{I}_1\otimes\mathbf{N}_2^{(2)}\otimes\mathbf{I}_3+k_{3,z}\cdot\mathbf{I}_1\otimes\mathbf{I}_2\otimes\mathbf{N}_3^{(1)}+k_3\cdot\mathbf{I}_1\otimes\mathbf{I}_2\otimes\mathbf{N}_3^{(2)}\Big][T]+Q\\&=\begin{bmatrix}0&\cdots&0\\\vdots&\ddots&\vdots\\0&\cdots&0\end{bmatrix},\end{aligned}\tag{3.15}$$

where $k_{1,x}$, $k_{2,y}$ and $k_{3,z}$ are equal to $\frac{dk_1}{dx}$, $\frac{dk_2}{dy}$, $\frac{dk_3}{dz}$, respectively, and $\mathbf{I}_1$, $\mathbf{I}_2$, $\mathbf{I}_3$ are the unit matrix with the size equal to m_1, m_2, m_3, respectively.

In this manner, the boundary conditions can be directly expressed as follows

the Dirichlet boundary condition:

$$[T]=\bar{T}.\tag{3.16}$$

the Neumann boundary condition:

$$\Big[k_1\cdot\mathbf{N}_1^{(1)}\otimes\mathbf{I}_2\otimes\mathbf{I}_3\cdot n_x+k_2\cdot\mathbf{I}_1\otimes\mathbf{N}_2^{(1)}\otimes\mathbf{I}_3\cdot n_y+k_3\cdot\mathbf{I}_1\otimes\mathbf{I}_2\otimes\mathbf{N}_3^{(1)}\cdot n_z\Big][T]=[\bar{q}].\tag{3.17}$$

the Robin boundary condition:

$$\begin{aligned}&\Big[k_1\cdot\mathbf{N}_1^{(1)}\otimes\mathbf{I}_2\otimes\mathbf{I}_3\cdot n_x+k_2\cdot\mathbf{I}_1\otimes\mathbf{N}_2^{(1)}\otimes\mathbf{I}_3\cdot n_y\\&\quad+k_3\cdot\mathbf{I}_1\otimes\mathbf{I}_2\otimes\mathbf{N}_3^{(1)}\cdot n_z+h\cdot\mathbf{I}_1\otimes\mathbf{I}_2\otimes\mathbf{I}_3\Big][T]=\big[h\cdot T_f\big].\end{aligned}\tag{3.18}$$

Since the tensor product possesses the characteristic of mapping the one-dimensional MLS shape function to the high-dimensional approximate solution space, the approximation functions of three-dimensional heat conduction problems are formulated by one-dimensional boundary shape functions in the BMC implementation. The approximation procedure is tremendously simplified since the coupling terms of the MLS basis function have been eliminated. Also, the three-dimensional weight functions are replaced by one-dimensional weight functions, which also greatly improve calculation efficiency. The difference between BMC and MLS is that the coupling terms (such as xy, xz, yz et al.) are eliminated in the BMC basis functions for three-dimensional problems, as shown in Table 1. Noted that the boundary shape functions are formally equal to the one-dimensional MLS approximation shape functions.

4 Numerical examples

Considering the numerical accuracy and efficiency of the BMC approach, four examples are investigated concerning heat conduction analysis. The relative error indicator of nu-

Table 1: The comparison between MLS and BMC methods for three-dimensional problems.

The order of the basis function	MLS	BMC
Linear	$1,x,y,z$	$1,x$ $1,y$ $1,z$
Quadratic	$1,x,y,z,xy,xz$ yz,x^2,y^2,z^2	$1,x,x^2$ $1,y,y^2$ $1,z,z^2$
Cubic	$1,x,y,z,xy,xz,yz,x^2,$ $y^2,z^2,xy^2,xz^2,x^2y,$ $x^2z,yz^2,y^2z,x^3,y^3,z^3$	$1,z,z^2$ $1,y,x^2,y^3$ $1,z,z^2,z^3$

merical results is employed as below

$$\text{Error}_{\text{L}_2}=\frac{\left\{\sum_{i=1}^{N}[\tilde{f}(i)-f(i)]^2\right\}^{\frac{1}{2}}}{\left\{\sum_{i=1}^{N}[f(i)]^2\right\}^{\frac{1}{2}}}, \tag{4.1}$$

where $\tilde{f}$ and f denote the numerical results and analytical results at the computational node, and N is the total number of computational nodes. The BMC method is compared with other methods on the 11$^{\text{th}}$ Gen Intel(R) Core(TM) i5-1130G7@ 1.80GHz,16GB RAM computer system. In addition, the FEM implementation is automatically completed by the COMSOL software.

4.1 Patch test

As a first example, a 2m$\times$1m plate, which exits the uniform heat source $Q=50\text{W}/\text{m}^2$ and the thermal conductivity is $k=1\text{W}/(\text{m}^\circ\text{C})$, as shown in Fig. 3. The upper and right boundaries are applied with the boundary condition $T=100^\circ\text{C}$, and the boundary conditions on the bottom and left boundaries are $T=0^\circ\text{C}$. The analytical temperature of this problem is defined as follows

$$T(x,y)=\frac{Q}{k\beta_m^3}\sum_{m=1}^{\infty}(-1)^m\frac{2}{a\cosh(\beta_m b)}\cosh(\beta_m y)\cosh(\beta_m x)+\frac{Q}{2k}\left(a^2-x^2\right)+T_w. \tag{4.2}$$

where $\beta_m=\frac{(2m-1)\pi}{2a}$, $m=1,2,\cdots,N$.

In the present computation, a uniform point distribution 41×21 is adopted by the BMC method as shown in Fig. 4(a). For comparison, the mesh distribution of 800 quadrilateral elements is used in FEM as shown in Fig. 4(b). The Quadratic basis function and Gauss weight function have been chosen to construct boundary shape functions.

It is evident from Fig. 5 that the numerical results of the BMC and FEM agree well with the results of analytical results. The relative error of the BMC and FEM are 1.57e-5 and

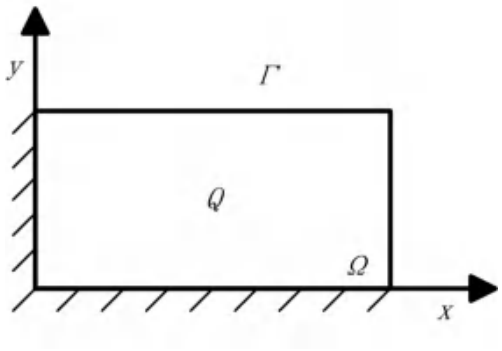

Figure 3: Problem description for a patch test.

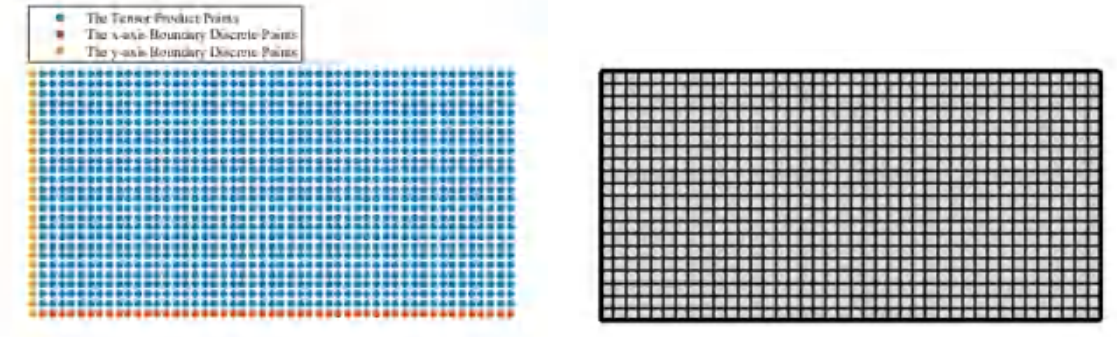

(a) BMC (b) FEM

Figure 4: Point distribution of plate with the BMC and FEM.

2.51e-5. Meanwhile, a more detailed comparison is shown in Fig. 6. It is illustrated that the optimized FEM results have similar accuracy for different discretization, however, the BMC method is more accurate than the FEM with a refinement of discretization. The convergence curve of the BMC numerical results with three different basis functions is shown in Fig. 7.

It can be observed that the quartic basis has a better performance than the quadratic and cubic basis functions. As for the stability analysis, it is presented in Fig. 8 that, as the number of discrete points on the boundaries increases, the largest condition number is obtained by the quartic basis function among these basis functions, which indicates the stability of the BMC approach decrease as the order of basis functions increases.

Furthermore, the convergence and stability study of the BMC method using three different weight functions is also presented in Fig. 9. It is evident that the numerical results obtained by the Gauss weight function are more refined than the cubic and quartic weight functions. Meanwhile, it is shown in Fig. 10 that the stability of the quartic spline weight function and the Gauss weight function is similar, and both are superior to the cubic spline functions. Synthesizes convergence and stability, the quadratic basis func-

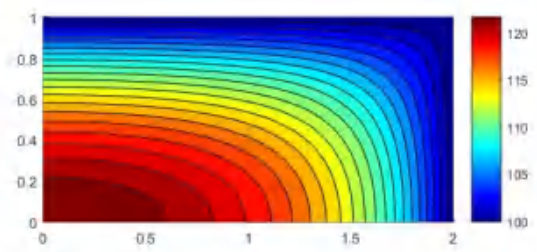

(a) Analytical solution

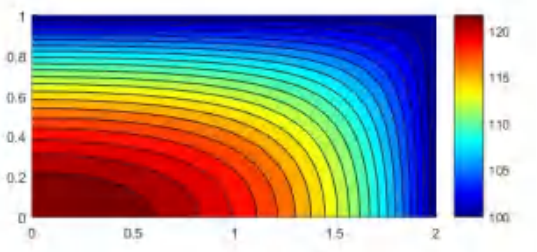

(b) BMC solution

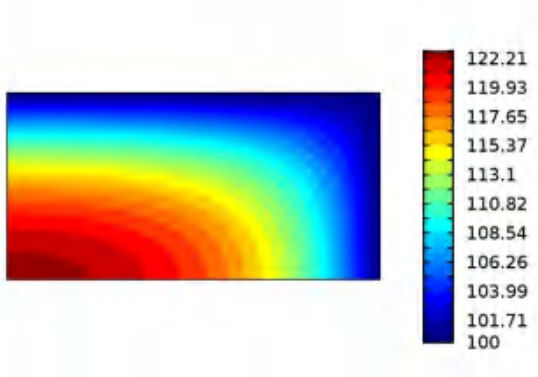

(c) FEM solution

Figure 5: Comparison of temperature field for the plate.

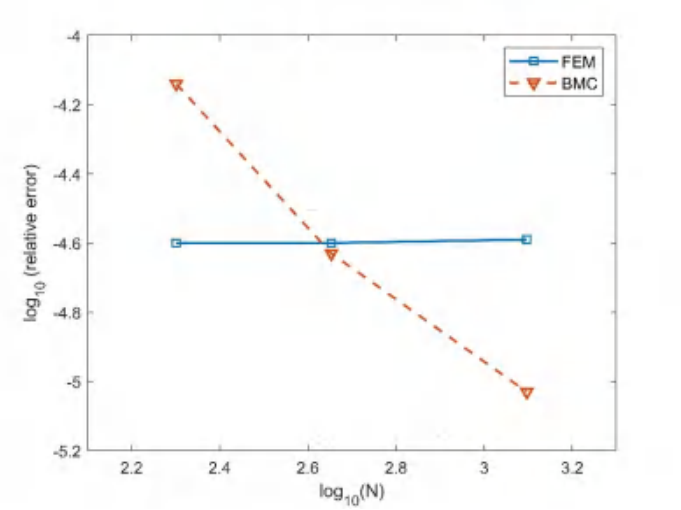

Figure 6: The relative error for the BMC and FEM, N is the number of computational points or mesh grids.

tion and the Gauss weight function will be used in the following three examples by the BMC implementation.

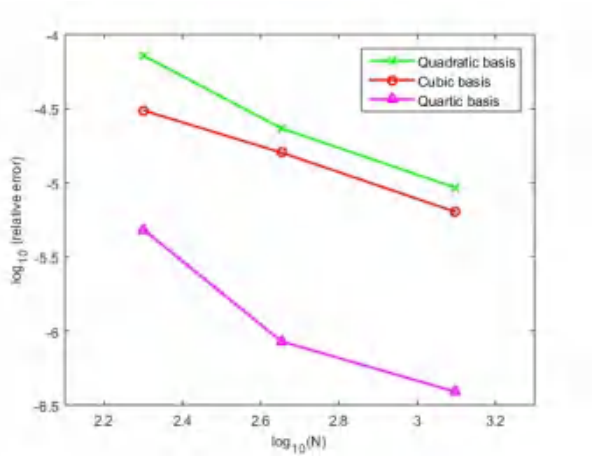

Figure 7: The relative error for the BMC results with different basis functions.

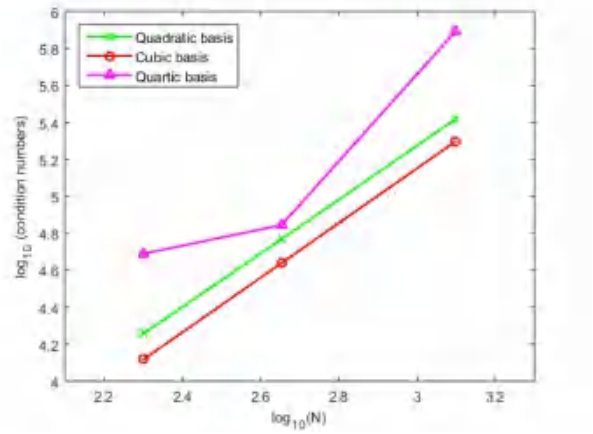

Figure 8: The conditional number for the stiffness matrix with different basis functions.

4.2 A square region with spatially varying conductivity

We consider an $L\times L$ plate with a nonuniformly distributed heat source and varying thermal conductivity along the x-axis (as seen in Fig. 11). The boundary condition on the top, bottom, left, and right boundaries are $T_t=0°\text{C}$, $T_b=0°\text{C}$, $T_l=0°\text{C}$ and $T_r=0°\text{C}$, respectively. The heat generation function is

$$Q(x)=\frac{x}{L}\left(1-\frac{x}{L}\right),$$

the thermal conductivity is $k(x)=\left(1+\frac{x}{L}\right)^3$, and the heat flux is

$$q(\boldsymbol{x})=-k(\boldsymbol{x})\frac{\partial T(\boldsymbol{x})}{\partial x}n(\boldsymbol{x}),\quad \boldsymbol{x}=x,y.$$

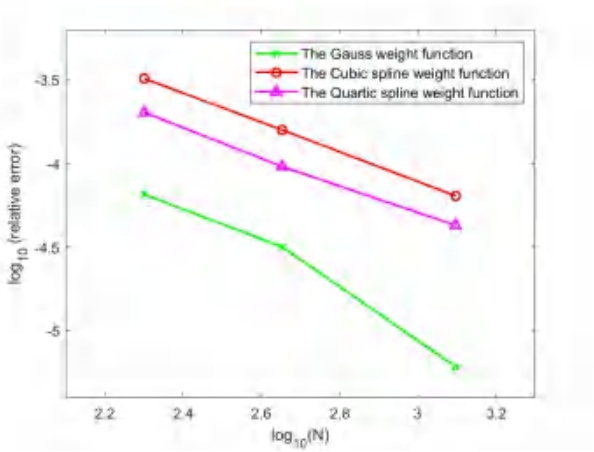

Figure 9: The relative error for the BMC results with different weight functions.

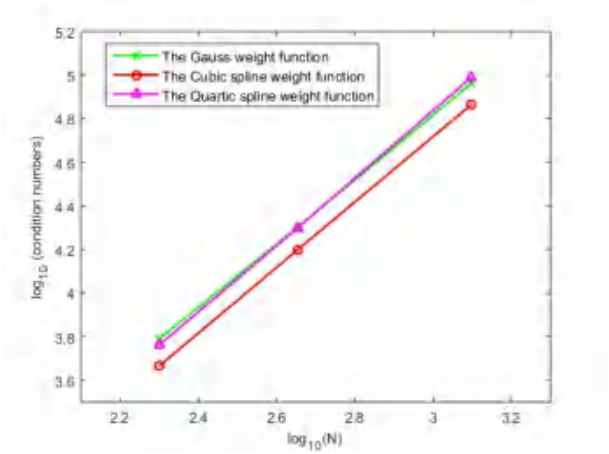

Figure 10: The conditional number for the stiffness matrix with different weight functions.

The analytical temperature (Gao 2006) is defined as

$$T(x)=\frac{100}{3}\left\{x-\frac{5000(950+3C_1+12x)}{(100+x)^2}-450\log(100+x)\right\}+C_2, \tag{4.3}$$

where

$$C_1=400\log(2)-\frac{2474}{9},$$
$$C_2=\frac{200}{9}\{103+2250\log(2)+1350\log(5)\}.$$

In this example, the uniform boundary discrete points $N_x=41$, $N_y=41$ are distributed in the x, y directions, respectively. For verifying the accuracy of the BMC method, numerical

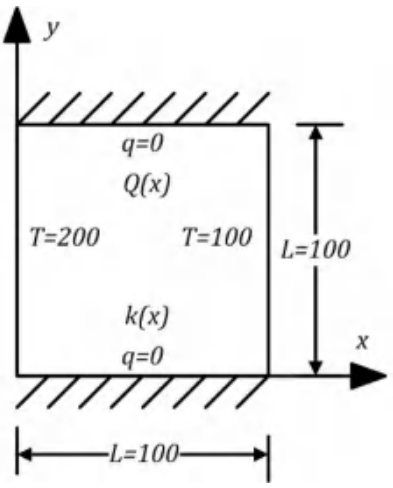

Figure 11: Square plate subjected to heat generator and varying conductivity.

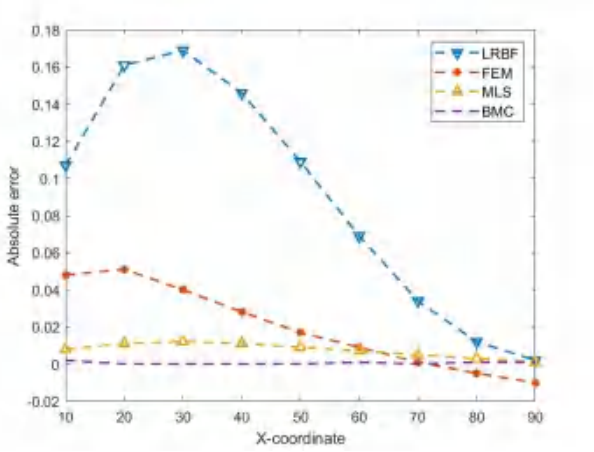

Figure 12: Computed temperature for the square plate with different methods for a square plate with spatial varying conductivity.

results along $y=50$ are compared with the exact solution are shown in Table 2 and Fig. 12. The numerical solution of the BMC approach is more precise than the local form of the MPCM, LRBF and FEM [27]. Moreover, Fig. 13 gives the comparison of time-consuming between the BMC and FEM methods, in which three discretization forms (21×21, 41×41, 61×61) are employed in examining the influence of discrete nodes on the computational efficiency, and it is evident that the BMC approach is more efficient than the FEM.

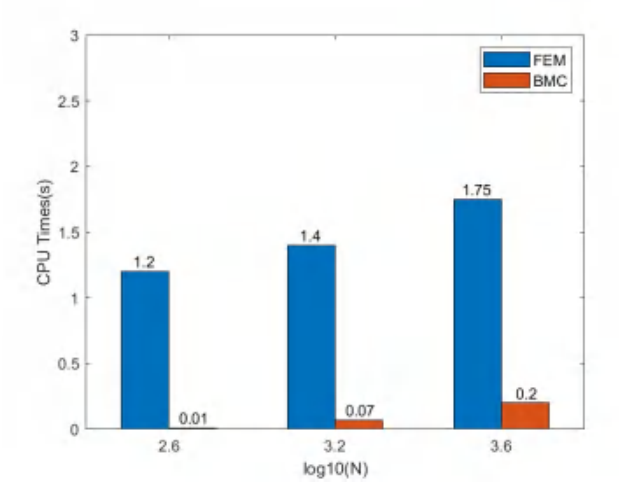

Figure 13: The comparison of time-consuming between the BMC and FEM for a square plate with spatial varying conductivity.

Table 2: Comparison of the BMC solution with LRBF, FEM, and exact solution (°C).

x	Exact	LRBF	FEM	MPCM	BMC
10	219.288	219.395	219.336	219.290	219.290
20	228.237	228.398	228.288	228.248	228.237
30	227.119	227.288	227.159	227.131	227.119
40	217.760	217.906	217.788	217.771	217.760
50	202.375	202.484	202.392	202.384	202.375
60	183.093	183.162	183.102	183.100	183.094
70	161.786	161.820	161.787	161.791	161.786
80	140.022	140.034	140.017	140.025	140.023
90	119.084	119.086	119.074	119.085	119.085

4.3 Heat transfer in the insulation of vapor transport tubes

In the present case, we considered that the pipe of vapor transport with a radius of 100mm was covered by the heat insulation layer, constructing a square structure of 400mm$\times$400mm, as shown in Fig. 14. The inner and outer surfaces of the thermal insulation layer are imposed with the temperatures $T_1=200^\circ$C and $T_2=20^\circ$C, respectively. And the heat conductivity is $k=0.1\mathrm{W}/(\mathrm{m}\cdot^\circ\mathrm{C})$.

The points distribution form of the BMC approach and the meshing scheme of the FEM are described in Fig. 15, and this two discretization are similar. The quadratic basis functions and the Gauss weight function are adopted for this example.

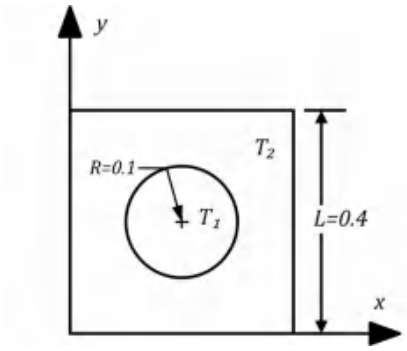

Figure 14: The physical model for insulation of tube transporting vapor.

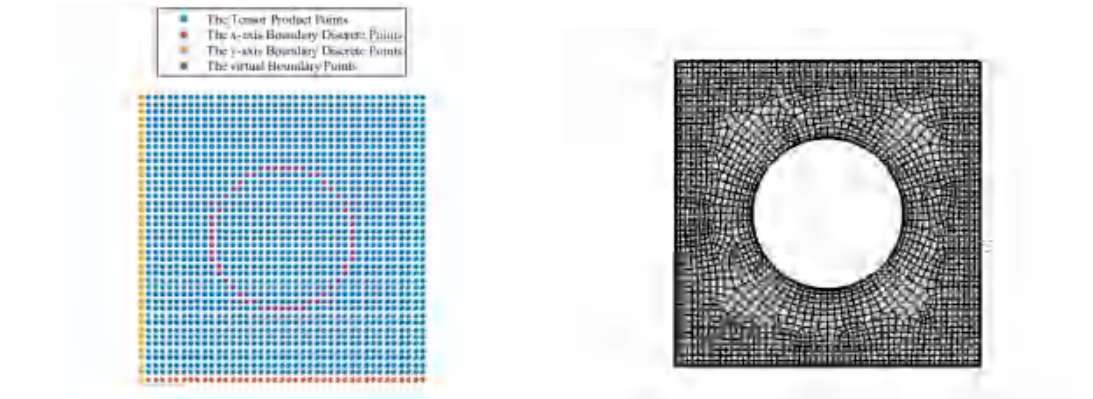

(a) BMC (b)FEM

Figure 15: Point distribution for insulation of tube transporting vapor with the BMC and FEM.

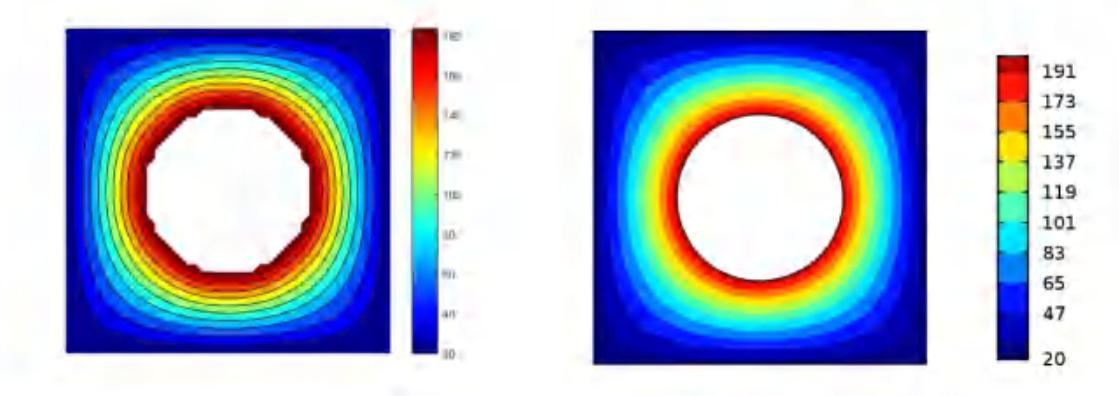

(a) BMC (b)FEM

Figure 16: Comparison of temperature field for insulation of tube transporting vapor with the BMC and FEM.

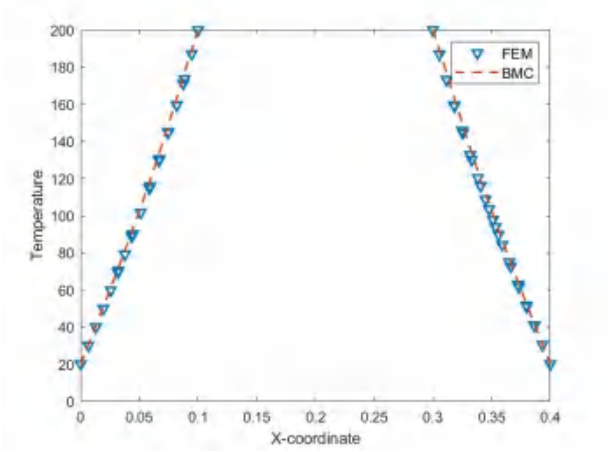

Figure 17: Computed temperature for insulation of tube transporting vapor at $y=0.2$.

4.4 Heat transfer in a three-dimensional irregular structure with varying thermal conductivity

In this example, a three-dimensional anisotropic heat conduction problem is considered. A three-dimensional domain is a $3\text{m}\times 3\text{m}\times 0.5\text{m}$ plate with a $1\text{m}\times 1\text{m}\times 0.5\text{m}$ square hole, the temperature of the inside surface, surrounding surfaces are $T_{in}=100^{\circ}\text{C}$ and $T_S=20^{\circ}\text{C}$ while the front and back surfaces are insulated $q(\boldsymbol{x})=0$, $\boldsymbol{x}=x,y,z$, as represented in Fig. 19. The varying thermal conductivities along the x,y,z-axis are $k(x)=e^{5x}\text{W}/(\text{m}\cdot^{\circ}\text{C})$, $k(y)=e^{5x}\text{w}/(\text{m}^{\circ}\text{C})$, $k(z)=e^{5x}\text{w}/(\text{m}^{\circ}\text{C})$, respectively. Fig. 20 presents the BMC and FEM discretization of the irregular structure. The number of BMC computational points is 1536, with uniform boundary discrete points $N_x=12$, $N_y=12$, $N_z=6$. In addition, 256 hexahedron elements, 384 tetrahedron elements, and 144 boundary elements are adopted in FEM.

Figs. 21 and 22 give predicted temperature fields and temperature distributions along line $y=1$, $z=0$ of the proposed method and FEM, respectively. From Fig. 23, we can see that the results of these two methods are quite close to each other. Nevertheless, it should be noted that the maximum relative error of 7% is concentrated near the inner corner. Additionally, the comparison of computational efficiency with discretization forms $12\times 12\times 6$,$21\times 21\times 6$ and $31\times 31\times 6$ between the BMC and FEM are displayed in Fig. 24. Overall, it can be evident that the BMC is more efficient for solving complex threedimensional thermal conduction problems.

5 Analysis and discussions

Findings in this paper illustrate that the BMC method has been well developed for steady-state heat conduction problems with spatially varying thermal conductivity prob-

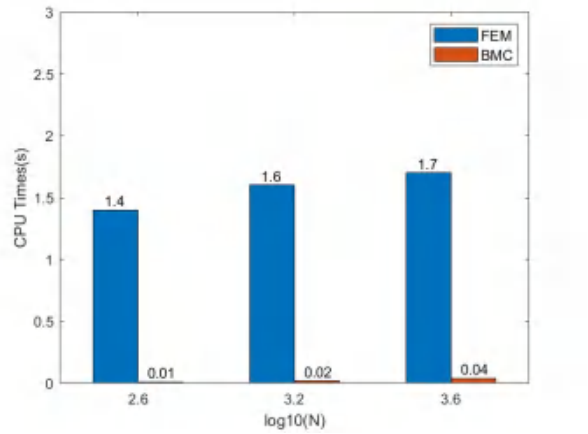

Figure 18: The comparison of time-consuming between the BMC and FEM for heat conduction in a square insulation layer of pipe.

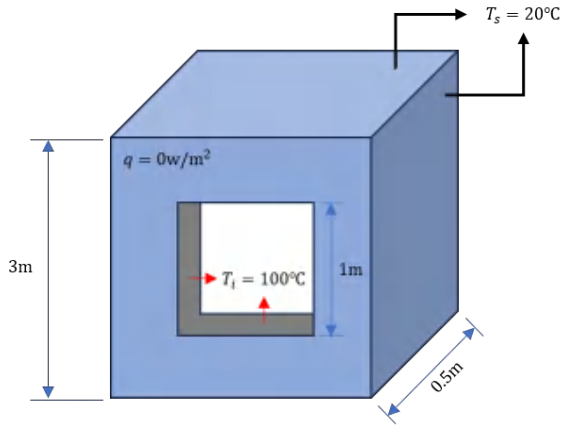

Figure 19: Geometry and parameters information of the 3D plate with a square hole.

lems. Due to the tensor product introduced, the high-dimensional heat conduction equations with complex boundary conditions have been successfully solved by one-dimensional shape functions. The effects of basis and weight functions on the BMC approach are shown in Figs. 7-10. It is noticeable that the high-order basis functions have positive effects on computational accuracy, while having negative effects on computational stability, and the Gauss weight function has a better performance than others regardless of accuracy or stability. This is mainly because the convergence rates of the MLS technique strongly depend on the radius of the support domain [24, 28]. Meanwhile, Huang et al. [24] have given a detailed analysis concerning the scale parameter c.

Fig. 12 shows that, among the LRBF, FEM and BMC methods, the most accurate

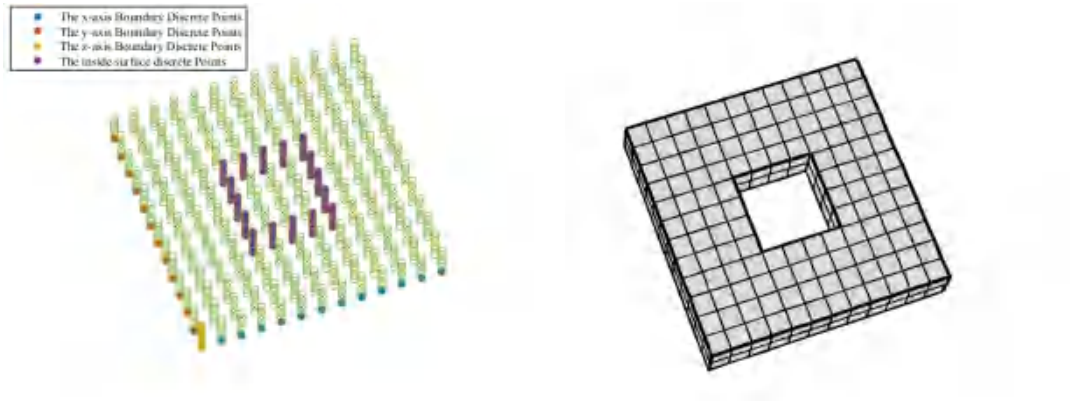

(a) BMC (b)FEM

Figure 20: Point distribution of 3D structure with the BMC and FEM.

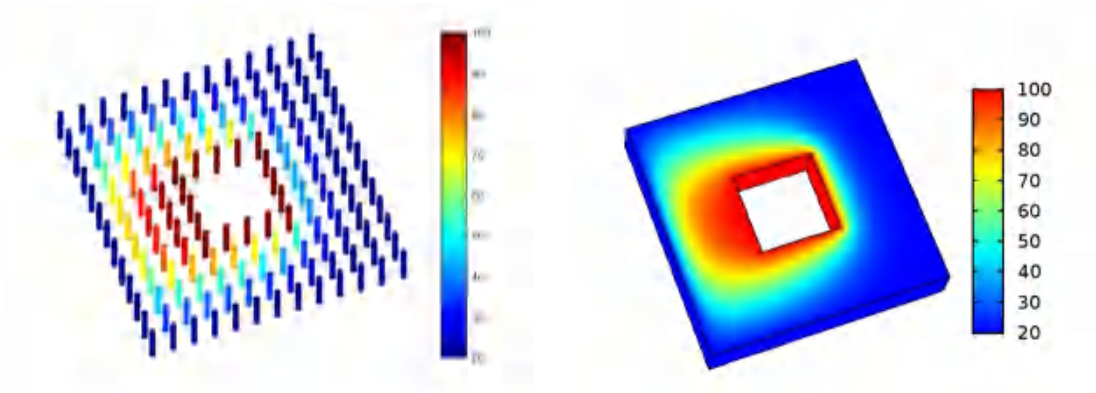

(a) BMC (b)FEM

Figure 21: Comparison of temperature field for insulation of 3D structure with the BMC and FEM.

results of the proposed approach for heat conduction problems with spatial varying conductivity can be obtained. Meanwhile, in contrast to the FEM which is implemented by the commercial program COMSOL, the proposed approach possesses less time-consuming within different discretization schemes. This characteristic of the BMC method with high efficiency is further certified in Example 3 and Example 4 for isotropy, anisotropy and complex boundary problems, especially concerning low-order basis functions. It may well be that, the small value of the scale parameter which is used for math with low-order functions, maintains the very limited bandwidth of the computation matrix.

To investigate the steady-state, anisotropic thermal conduction problem, discretization types of the BMC and FEM within a three-dimensional irregular domain are performed in Fig. 20. Fig. 21 verify the applicability of the BMC method to steady-state,

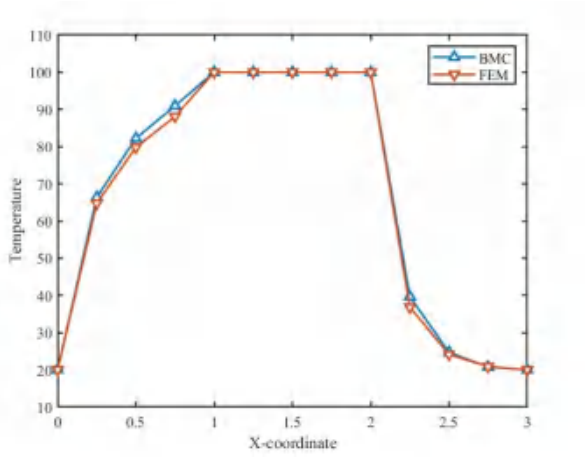

Figure 22: Computed temperature for insulation of 3D structure along line $y=1$, $z=0$.

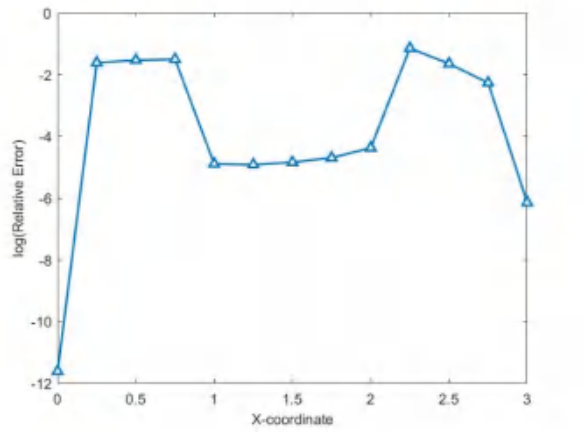

Figure 23: Relative error along line $y=1$, $z=0$.

anisotropic heat conduction problems, since the BMC results are well in agreement with the FEM. In particular, by contrast, Fig. 24 indicates that the BMC method possesses a higher efficiency than the FEM for solving complex heat conduction. Previous research on heat conduction showed that the application of the meshfree method had been restricted due to the computational efficiency and complexity. The major differences within the present work from previous studies, e.g., Chen et al. [29], Fu et al. [30] are as following. First, there are no elaborate mesh and integrations on the boundary or in the domain. Second, by introducing the tensor product, the two or three-dimensional heat conduction equations are approximated by one-dimensional boundary shape functions. Hence, in comparison with existing methods for solving heat conduction problems, the proposed method has the well potential to become an attractive alternative to the tradi-

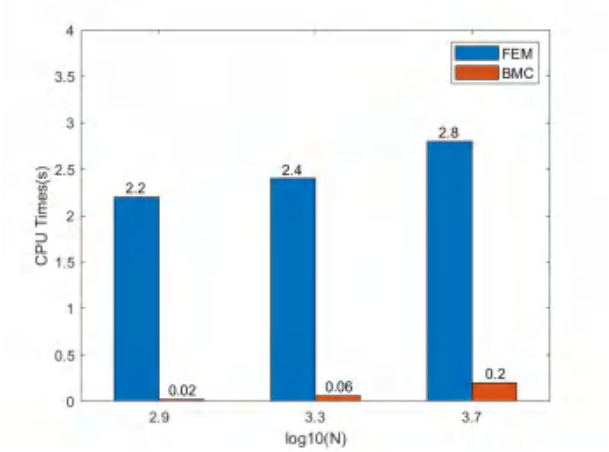

Figure 24: The comparison of time-consuming between the BMC and FEM for three-dimensional complex heat conduction problem.

tional methods.

In this work, the BMC approach has been developed for three-dimensional steady-state heat conduction problems with spatially varying thermal conductivity. The 1D moving least squares and the Kronecker product are used for the BMC approximation of the two/three-dimensional temperature fields. Due to the features of these two approaches, the complex shape functions have been simplified to 1D shape functions for 2D and 3D heat conduction problems. However, due to the complexity of the spatial structures of high-performance materials within engineering practice, the errors of the BMC results which are near the boundary are needed to reduce. In addition, this work is restricted to steady-state and small-scale configurations, further efforts of transient state and large-scale computation are to be continued.

6 Conclusions

The conclusions of this paper are summarized as follows:

- In this study, the BMC method is proposed to investigate nonhomogeneous thermal conduction problems by combing the one-dimensional MLS technique and the tensor product.
- With increasing the order of basis function the computational accuracy increase and the computational stability decrease. The Gauss weight function is the most suitable choice in the present work regardless of accuracy or stability.
- The proposed approach possesses a very high efficiency in this study for solving two-dimensional and three-dimensional anisotropic heat conduction problems with complex boundaries by comparing the BMC results with the FEM solutions.

Acknowledgements

This work is supported by GuangDong Basic and Applied Basic Research Foundation (No. 2021A1515110807), the PhD Starting Foundation of Nanchang Hangkong University (No. EA202411285), the Program for Guangdong Introducing Innovative and Entrepreneurial Teams (No. 2019ZT08G315) and National Natural Science Foundation of China (No. U19A2098).

References

[1] W. TAO, Numerical Heat Transfer, Second ed., Xi'An Jiaotong University Press, Xi'An, 2001.
[2] R. LEWIS, P. NITHIARASU AND K. SEETHARAMU, Fundamentals of the Finite Element Method for Heat and Fluid Flow, Chichester, England: Wilry, 2004.
[3] H. HUANG AND A. USMANI, Finite Element Analysis for Heat Transfer: Theory and Software, London: Springer-Verlag, 1994.
[4] M. A. AL-JAWARY, J. RAVNIK, L. C. WROBEL, AND L. SKERGET, *Boundary element formulations for the numerical solution of two-dimensional diffusion problems with variable coefficients,* Comput. Math. Appl., 64 (2012), pp. 2695–2711.
[5] A. GOSH AND S. MUKHERJEE, *Boundary element method analysis of thermoelastic deformation in nonhomogeneous media,* Int. J. Solids Struct., 20(9) (1984), pp. 829–843.
[6] R. BIALECKI AND G. KHUN, *Boundary element solution of heat conduction problems in multizone bodies of nonlinear materials,* Int. J. Numer. Meth. Eng., 36 (1993), pp. 799–809.
[7] J. SLADEK, V. SLADEK AND S. ATLURI, *Local boundary integral equation (LBIE) method for solving problems of elasticity with nonhomogeneous material properties,* Comput. Mech., 24 (2000), pp. 456–462.
[8] E. DIVO AND A. KASSAB, Boundary Element Methods for Heat Conduction: with Applications in Non-homogeneous Media, WIT Press: Southampton, 2003.
[9] M. NGUYEN, AND T. BUI, ET AL., *Enhanced nodal gradient 3D consecutive-interpolation tetrahedral element (CTH4) for heat transfer analysis,* Int. J. Heat Mass Trans, 103 (2016), pp. 14–27.
[10] Z. AN AND T. YU ET AL., *Implementation of isogeometric boundary element method for 2-D steady heat transfer analysis,* Adv. Eng. Software, 116 (2018), pp. 36–49.
[11] X. GAO, *A meshless BEM for isotropic heat conduction problems with heat generation and spatially varying conductivity,* Int. J. Numer. Methods Eng., 66(2006), pp. 1411–1431.
[12] K. YANG AND X. GAO, *Radial integration BEM for transient heat conduction problems,* Eng. Anal. Boundary Elem., 34 (2010), pp. 557–563.
[13] A. SINGH. I. SINGH AND R. PRAKASK, *Meshless element free Galerkin method for unsteady nonlinear heat transfer problems,* Int. Heat Mass Trans., 50 (2007), pp. 1212–1219.
[14] X. ZHANG, P. ZHANG AND L. ZHANG, *An improved meshless method with almost interpolation property for isotropic heat conduction problems,* Eng. Anal. Boundary Elem., 33 (2013), pp. 850–859.
[15] M. CUI, H. PENG AND B. XU ET AL., *A new radial integration polygonal boundary element method for solving heat conduction problems,* Int. J. Heat Mass Trans., 123 (2018), pp. 251–260.
[16] X. WU AND W. TAO, *Meshless method based on the local weak-forms for steady-state heat conduction problems,* Eng. Anal. Boundary Elem., 34 (2010), pp. 557–563.
[17] Z. LI, Z. CHEN, X. WU AND W. TAO, *Coupled MLPG-FVM simulation of steady state heat conduction in irregular geometry,* Eng. Anal. Boundary Elem., 100 (2019), pp. 265–275.

[18] S. ATLURI AND S. SHEN, *The meshless local Petrov–Galerkin (MLPG) method: a simple and less costly alternative to the finite element and boundary element methods.,* Comput. Model Eng. Sci., 3 (2002), pp. 11-–52.
[19] S. ATLURI AND S. SHEN, The Meshless Local Petrov–Galerkin (MLPG) Method, Encino, CA: Tech Science Press, 2002.
[20] S. ATLURI AND S. SHEN, The Meshless Method (MLPG) for Domain & BIE Discreations, Forsyth, GA: Tech Science Press, 2004.
[21] X. WEI, W. CHEN, B. CHEN AND L. SUN, *Singular boundary method for heat conduction problems with certain spatially varying conductivity,* Comput. Math. Appl., 69 (2015), pp. 206–222.
[22] Y. DAI, X. WU AND W. TAO, *Weighted least-squares collocation method (WLSCM) for 2-D and 3-D heat conduction problems in irregular domains,* Numer. Heat Transf. B., 59 (2012), pp. 473-–494.
[23] Z. HUANG, D. LEI AND Y. WANG, *Modified moving least square collocation method for solving wave equations,* Adv. Appl. Math. Mech., 10 (2019), pp. 1–17.
[24] Z. HUANG, D. LEI, D. HUANG, J. LIN AND Z. HAN, *Boundary moving least square method for 2D elasticity problems,* Eng. Anal. Bound. Elem., 106 (2019), pp. 505–512.
[25] Z. HUANG, D. LEI, Z. HAN, P. ZHANG, *Boundary moving least square method for numerical evaluation of two-dimensional elastic membrane and plate dynamics problems,* Eng. Anal. Bound. Elem., 108 (2019), pp. 41–48.
[26] Z. HUANG, L. DONG, Z. HAN AND J. LIN, *Boundary moving least square method for 3D elasticity problems elasticity problems,* Eng. Anal. Bound. Elem., 121 (2020), pp. 255–266.
[27] E. D. SKOURAS, G. C. BOURANTAS, V. C. LOUKOPOULOS, G. C. NIKIFORIDIS, *Truly meshless localized type techniques for the steady-state heat conduction problems for isotropic and functionally graded materials,* Eng. Anal. Bound. Elem., 35 (2011), pp. 452–464.
[28] T. BELYTSCHKO, Y. Y. LU AND L. GU, *Element-free Galerkin methods,* Int. J. Numer. Methods Eng., 37 (1994), pp. 229–256.
[29] B. CHEN, W. CHEN, ALEXANDER H. D. CHENG, AND X. WEI, *The singular boundary method for twodimensional static thermoelasticity analysis,* Comput. Math. Appl., 72 (2016), pp. 2716–2730.
[30] Z. FU, L. YANG, Q. XI, AND C. LIU, *A boundary collocation method for anomalous heat conduction analysis in functionally graded materials,* Comput. Math. Appl., 88 (2020), pp. 91–109.